EFFICIENCY CALIBRATION OF A NEUTRON LONG COUNTER

by

TRACY LYNN MacFARLANE

B.Sc., The University of New Brunswick, 1965

A THESIS SUBMITTED IN PARTIAL FULFILMENT OF

THE REQUIREMENTS FOR THE DEGREE OF

MASTER OF SCIENCE

in the Department

of

PHYSICS

We accept this thesis as conforming to the
required standard

THE UNIVERSITY OF BRITISH COLUMBIA

May, 1968

In presenting this thesis in partial fulfilment of the requirements

for an advanced degree at the University of British Columbia, I agree

that the Library shall make it freely available for reference and

Study. I further agree that permission for extensive copying of this

thesis for scholarly purposes may be granted by the Head of my

Department or by his representatives. It is understood that copying

or publication of this thesis for financial gain shall not be allowed

without my written permission.

Department of _Physics_

The University of British Columbia
Vancouver 8, Canada

Date _May 28, 1968_

ABSTRACT

The U.B.C. Hanson-McKibben type Long Counter has been modified to permit insertion of a larger diameter BF_3 proportional counter. An investigation was made to determine the effects of the modification on the neutron detection characteristics of the counter. 2.60 MeV and 3.09 MeV neutrons were obtained from the reaction $D(d,n)^3He$ and 4.5 MeV neutrons from a standard $^{241}AmBe$ source.

The efficiency of the Long Counter was determined in terms of counting rate per unit neutron flux occurring at the effective centre of the counter. The count rate used was that due to the $^{10}B(n,\alpha)^7Li$ pulses from the BF_3 counter located in the centre of the Long Counter. The effective centre was defined as that point inside the counter such that the counting rate varied as the inverse square of the distance of the source from the effective centre. The following table lists the neutron energy, efficiency and distance from the front reference face of the Long Counter to the effective centre.

Neutron Energy MeV	Efficiency counts / neutron per cm^2 at the effective centre	Distance to Effective Centre cm
2.580 (±.06%)	26.6 (±20%)	12.6 (±9%)
3.004 (±.3%)	29.4 (±19%)	10.3 (±7%)
4.5 (±10%)	14.1 (±2.2%)	10.8 (±6%)

The efficiency for 4.5 MeV neutrons was found to have increased

by at least an order of magnitude from that of the original Long Counter. However, the dependence of the efficiency on energy has been increased, varying by 50% over the range of energies measured.

The shielding on the sides of the Long Counter was found to reduce the intrinsic efficiency for neutrons incident from the side to 0.4 of that for neutrons incident on the front face.

TABLE OF CONTENTS

LIST OF FIGURES

ACKNOWLEDGEMENTS

CHAPTER I

INTRODUCTION

1.1. General Introduction

The Hanson-McKibben (1947) Long Counter developed at Los Alamos is probably the most widely used of all neutron detectors.

It consists of a long BF_3 proportional counter placed in a cylindrical moderator of paraffin. The moderator is surrounded all but on one end by a thermal neutron absorber, usually a thin sheet of cadmium, and a second fast neutron moderating layer surrounds the absorber. Neutrons incident on the open end are thermalized in the center moderator and have a high probability of entering the BF_3 counter, where they produce $^{10}B(n,\alpha)^7Li$ reactions in the counter gas. In general the gas is enriched to about 90% in ^{10}B, compared to the 19.8% of ^{10}B found in natural boron. Ions produced by the charged particles from the reactions are collected and produce an electrical pulse which is amplified and counted electronically. Neutrons incident from the side are largely thermalized in the outer moderator and either escape or are captured in the absorber. Therefore they have a small probability of entering the center region and do not contribute signficantly to the counting rate. Thus, the counter has the highest sensitivity only to those neutrons that enter the center region at one end.

Pangher and Nichols (1966) at the Pacific Northwest Laboratory in Richland, Washington have made an improvement by replacing the paraffin

with polyethylene, supported by aluminum rather than steel used by McKibben. The result was a highly reproducible detector with considerably better resolution on the neutron peak than the McKibben model.

The Long Counter is much used in the neutron range from 25 keV to 14 MeV. The absolute calibration is usually based on observing the counting rate for a neutron source with a known neutron output. Standard neutron sources are made of a natural or artificially produced alpha-emitter intimately mixed with beryllium in which the neutron yield arises from the reaction $^9Be(\alpha,n)^{12}C$. Typical sources such as Ra-Be or ^{241}Am-Be produce a broad spectrum of neutrons from a few MeV to 10 or 11 MeV, with a tendency to peaking in the 3 to 6 MeV range. This provides a reasonable calibration over the energy range in which the counters are used because the neutron detection efficiency of the counter with the usual dimensions is relatively independent of neutron energy. (Hanson and McKibben, 1947; Pangher and Nichols, 1966)

The original U.B.C. Long Counter was constructed by Heiberg (1954) using a Chalk River one inch diameter BF_3 counter. In 1966, when the counter began to fail, a decision was made to introduce gas counters of larger diameter and higher pressure containing either BF_3 or ^3He. The aim of the present work was to investigate the properties of these counters and in particular to make a more accurate measurement of the absolute efficiency for neutron detection using both accurately calibrated neutron sources and monoenergetic neutrons produced by the Van de Graaff generator. Using monoenergetic neutrons from reactions of known cross section in has been possible to investigate the efficiency of the detector

as a function of neutron energy.

A major disadvantage with the Long Counter is its slow response to incoming neutrons, making it of little use in time of flight or concidence measurements. In these cases a scintillation detector is often used. This type of detector consists of a scintillating material mounted on a photomultiplier. Some materials used are ^{6}Li-I(Tl) crystal, ^{6}Li loaded glass, a compound of 15% Zn-S activated with silver and dispersed in lucite (Hornyak 1952), and various liquid and plastic scintillators. These however require elaborate pulse shape analysis to separate the pulses originating from neutrons and those originating from gamma ray flux.

The major advantege of the Long Counter, its relatively constant efficiency with varying energy, is not always a desirable feature. Such a case is health monitoring of neutrons. The relative health hazard for a given flux of neutrons increases with energy. It was found by Bramlett, Ewing and Bonner (1960) that a ^{6}Li-I(Eu) crystal placed in the center of a 12 inch polyethylene sphere exhibited an efficiency variation with energy of the incident neutrons which closely approximated the energy variation of the health hazard of neutrons.

1.2. The Long Counter

The Long Counter depends on the detection of the alpha particles emitted by the reaction $^{10}B(n,\alpha)^7Li$ produced in boron trifluoride gas in a cylindrical proportional counter. The energy release in the reaction $^{10}B(n,\alpha)^7Li$ is 2.79 MeV. This is considerably greater than the energy lost by electrons traversing the counter volume. Proportional operation then ensures that processes leading to a single electron ejection, such as gamma interactions, produce pulses considerably smaller than the reaction pulses. This is important for a neutron detector since a neutron flux is often accompanied by a large gamma ray flux.

Table 1 shows the cross section of the reaction $^{10}B(n,\alpha)^7Li$ as taken from Hughes and Schwartz (1958).

TABLE 1

$^{10}B(n,\alpha)^7Li$ Cross Sections

Neutron Energy	Cross Section
0.0235 eV	3820 barns
6.0 eV	85 barns
10.0 keV	7 barns

Clearly the efficiency of the proportional counter depends strongly on the energy of the incident neutrons. The counter developed by Hanson and McKibben (1947) had a paraffin moderator arrangement to give a counting rate, as nearly as possible, proportional to the incident neutron flux and independent Of the neutron energy. By making the moderator appreciably longer than the mean free path of fast neutrons, neutrons
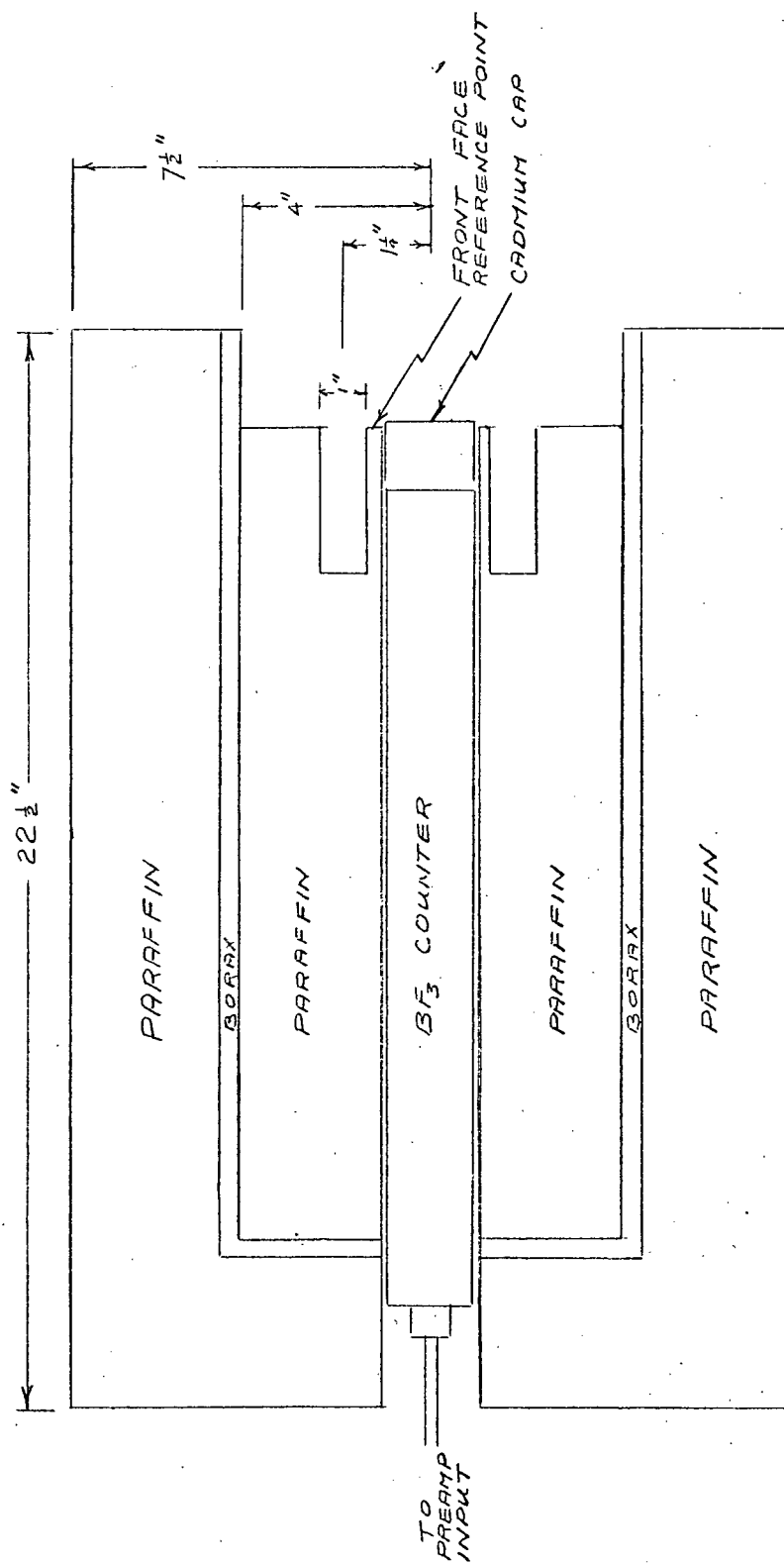
FIGURE 1. U.B.C. Long Counter

entering the moderator are slowed by successive collisions in the moderator so that the fraction that drifts into the counting tube at thermal energies varies little with energy.

The U.B.C. Long Counter, shown in Fig. 1, is based on the Hanson - McKibben design, however the present version has a larger BF_3 counter(2 inches in diameter) filled to 70 cm of Hg with 96% ^{10}B enriched BF_3. Further details concerning the counter and operating conditions are given in the Appendix.
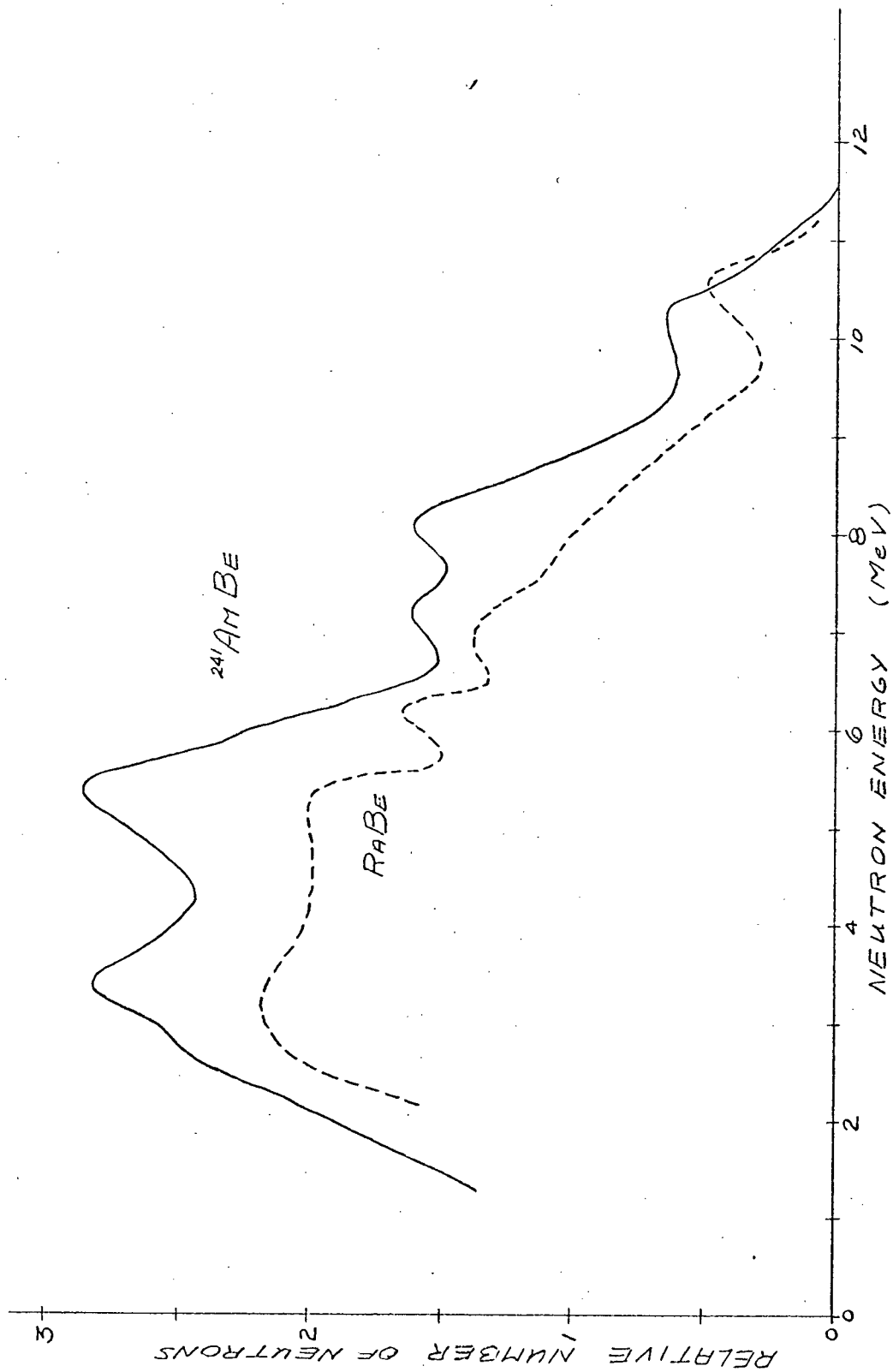
FIGURE 2. COMPARISON OF AmBe AND RaBe SPECTRA.

CHAPTER II

MEASUREMENT OF THE LONG COUNTER EFFICIENCY
USING AN ^{241}Am-Be NEUTRON SOURCE

2.1. The Standard Neutron Source

The efficiency of the long counter shown in Fig. 1 was measured using an accurately calibrated neutron source placed at various distances from the counter ranging from 10 cm to 150 cm.

The neutron source (type AMN-18) obtained from the Radiochemical Center, Amersham, England consisted of the alpha-emitter Americium-241 fused with beryllium metal. It produces neutrons by the reaction ^{9}Be$(\alpha,n)^{12}$C. The absolute neutron output was measured by K.W. Geiger at the National Research Council of Canada by a direct intercomparison with the Canadian Standard source #118 using a Precision Long Counter (Pangher and Nichols 1966). The Canadian standard had been absolutely calibrated by the manganese bath method (Geiger and Baerg, 1965), and intercompared with the standards of other countries. The neutron output for the present source was 7.62×10^5 ($\pm 2\%$) neutrons per second. (Calibration Report APXNR-2095, January 1968)

Some data on the alpha particles emitted by ^{241}Am and on the γ-rays from the daughter product ^{237}Np are given in Table 2 with the strongest lines underlined. The neutron energy spectrum is compared with that from a Ra-Be source in Fig. 2.

TABLE 2

$$^{241}\text{Am} \rightarrow \alpha + {}^{237}\text{Np} \ (T_{\frac{1}{2}} = 458 \text{ years})$$
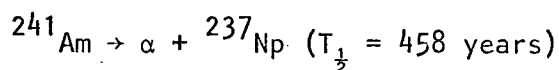
	α-Energy MeV	%	γ-Energy (%) MeV
α_0	5.545	0.25	0
α_{33}	5.513	0.12	0.0332 (100)
α_{60}	<u>5.486</u>	85.5	<u>0.0594 (94)</u>
			0.026 (6)
α_{103}	<u>5.443</u>	12.7	0.1029 (22)
			0.043 (78)
α_{159}	5.389	1.3	0.125 (11)
			0.099 (50)
			0.055 (39)

plus 18 other alpha groups, all less than 0.02%.

The complex alpha spectrum, combined with the fact that alpha particles of all energies slowing down in the source can produce neutrons which leave ^{12}C either in the ground state or in the first excited state at 4.43 MeV, gives rise to a broad neutron energy spectrum.

2.2. Measurements
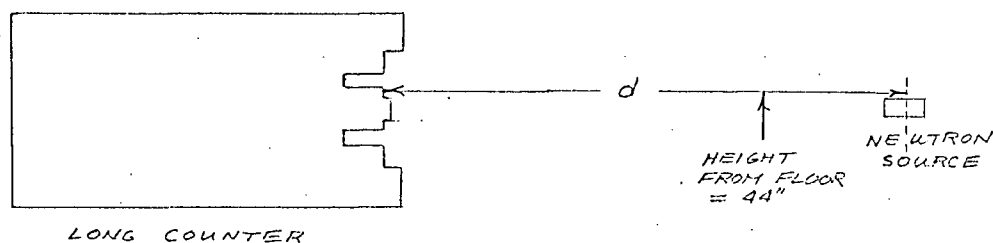

Figure 3. Arrangement of Long Counter and Neutron Source.

The Long Counter and source were arranged as shown in Figure 3, such that wall scattering of the neutrons was much less than scattering from the floor. The pulses from the Long Counter were analyzed in an ND-101 256 channel kicksorter, using the amplification system described
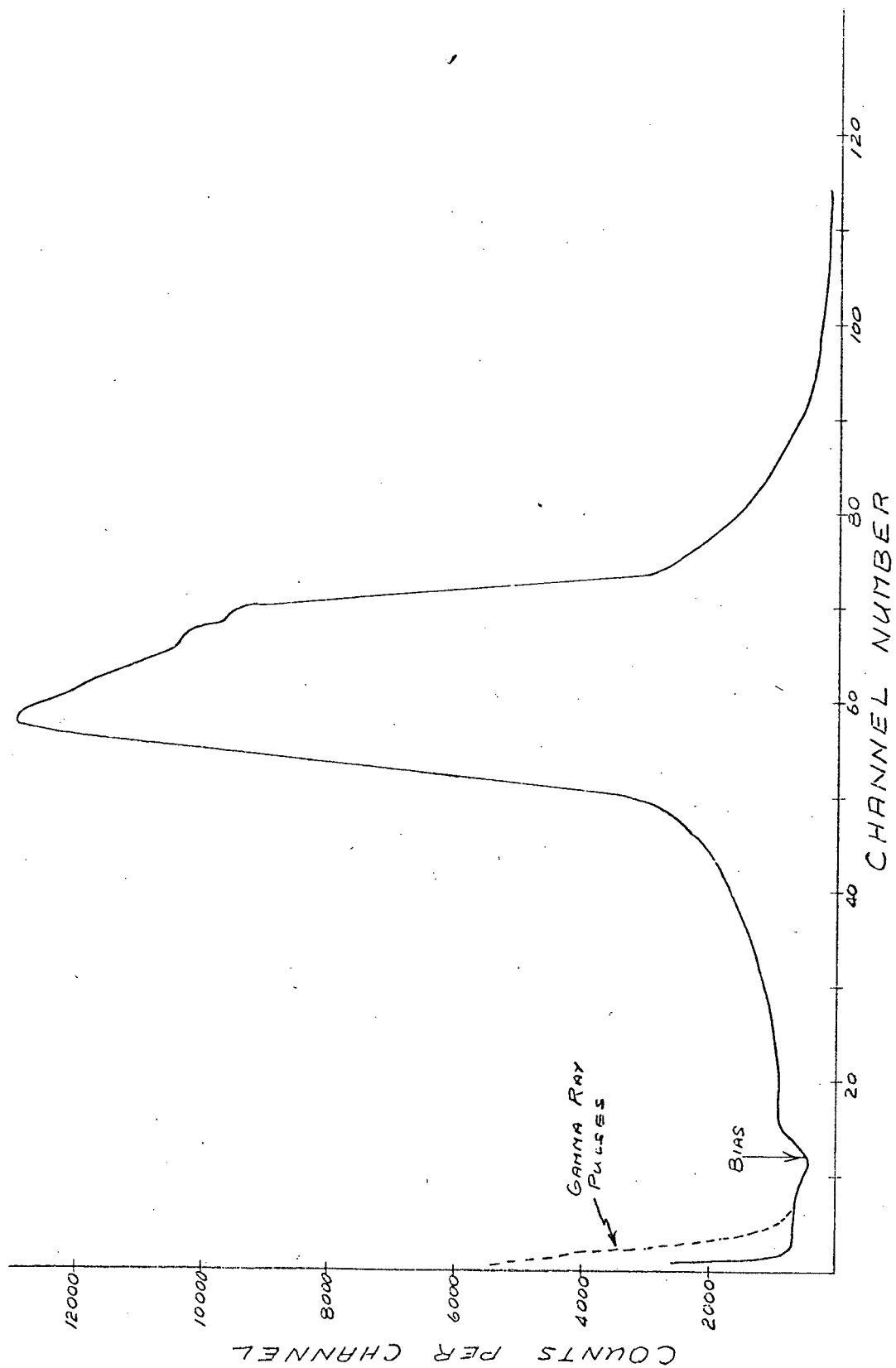
FIGURE 4. TYPICAL LONG COUNTER NEUTRON SPECTRUM

in Appendix A.1.

A typical neutron spectrum is shown in Figure 4. This spectrum resulted from a 30 minute exposure of the Long Counter to the Am-Be source at a distance d=60 cm.

The lop-sided appearance of the peak is explained by Pangher and Nichols (1966) in their work on an accurately reproducable long counter using polyethylene rather than paraffin. Their Precision Long Counter had better resolution than the Hanson-McKibben type; as a result two distinct peaks, a main peak and a smaller one at slightly higher energy, could be clearly resolved. The main peak was attributed to the case when the alpha particle from the reaction $^{10}B(n,\alpha)^{7}Li$ (Q = 2.31 MeV) leaves the ^{7}Li nucleus in its first excited state (478 keV above the ground state), and the second small peak, which produces the hump on the high energy side of Figure 4, to the case when the ^{7}Li nucleus is left in the ground state (Q = 2.79 MeV) (about 5% of the time).

To determine the number of counts in the spectrum due to neutrons, the background was subtracted and the spectrum integrated from a bias level to the point where the spectrum returned to background level.

So as to make the operation independent of the particular neutron source being used, a bias level was chosen to cut off all pulses resulting from gamma rays. This gives a bias unnecessarily high for such sources as Am-Be which produce little accompanying gamma flux, however it is appropriate for the many high gamma flux situations in which the counter may be used in future.

The bias was determined by running a spectrum similar to the Am Be one of Fig. 4. but using a Ra Be source with neutron flux of 7.5×10^5 neutrons per second accompanied by a high gamma flux. The spectrum was similar to that for Am Be but with a very high low energy tail, as dotted in on Fig. 4.

The effectiveness of the shielding layers around the sides of the Long Counter was investigated by determining the efficiency of the Long Counter for neutrons from the Am Be neutron source placed at various distances along a line at right angles to the axis of the Long Counter. The arrangement is shown in Fig. 5.
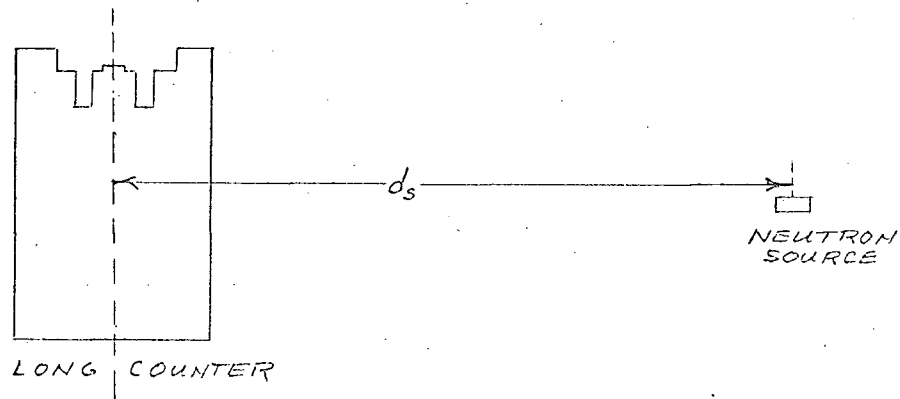

Figure 5. Arrangement of Long Counter and neutron source for shielding effectiveness investigation.
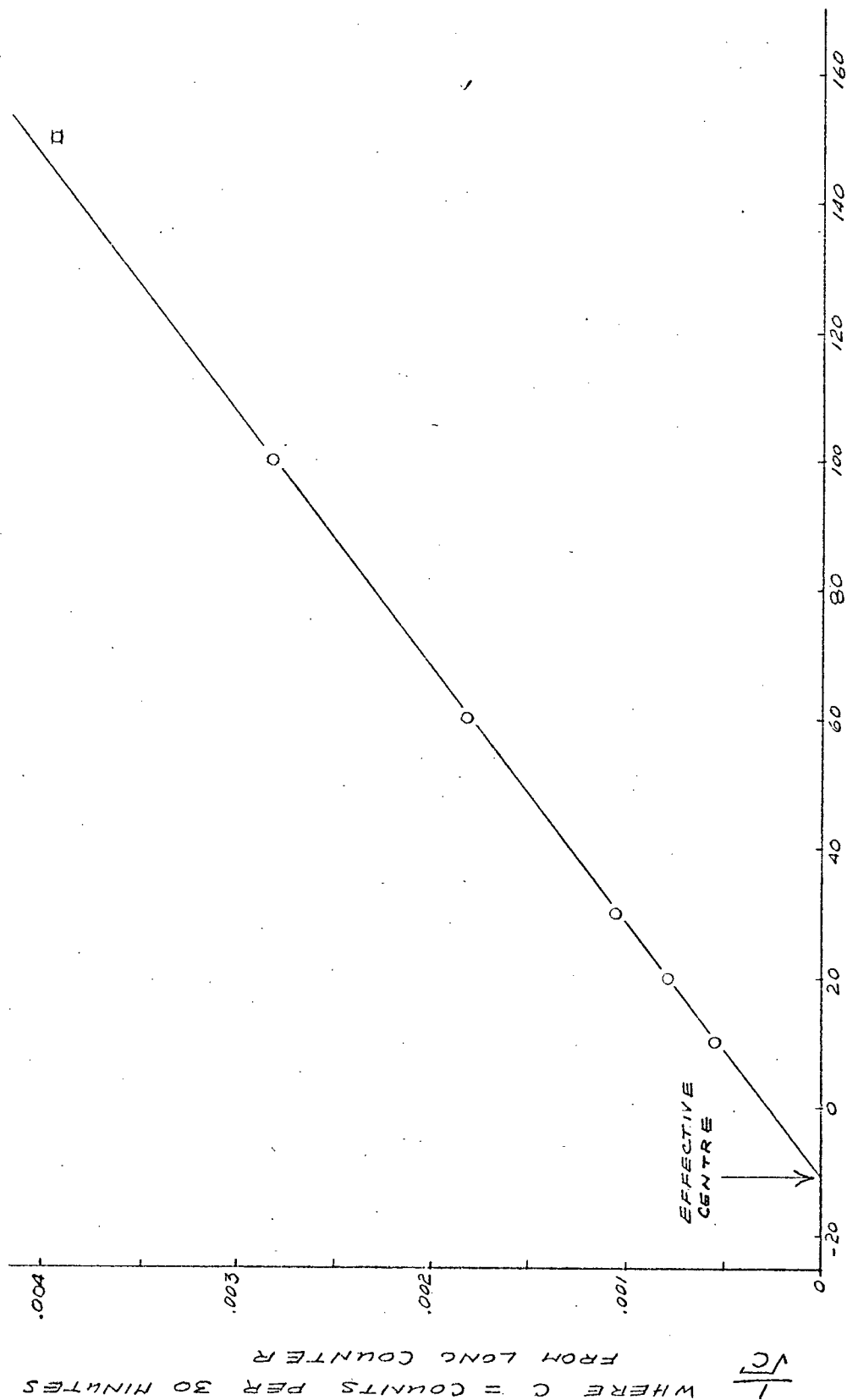
FIGURE 6. INVERSE SQUARE PLOT FOR Am Be CALIBRATION.

DISTANCE FROM LONG COUNTER FRONT FACE TO SOURCE (CM)

$\frac{1}{\sqrt{C}}$

WHERE C = COUNTS PER 30 MINUTES FROM LONG COUNTER

EFFECTIVE CENTRE

2.3. Calculation of Efficiency

In order to define an efficiency independent of the distance from the source to the Long Counter, a plot of $C^{-\frac{1}{2}}$ against the distance from the counter face to the source was made as shown in Fig. 6, where C is the count rate from the Long Counter. In the range of distances $d \leqslant 100$ cm this produced a reasonable approximation to a straight line. Beyond this point the room scattered neutron background became significant as indicated by the deviation of the data from the inverse square law. This line was extrapolated back to cross the distance axis at a point "e" cm from the origin, called the effective centre.

The Long Counter count rate can be related to its intrinsic efficiency and the neutron source strength as follows:

$$C = n \left[\frac{A}{4\pi \ (d+e)^2} \right] \varepsilon = n \frac{Eff}{4\pi D^2}$$

where: C = counts per unit time from Long Counter.
   n = neutrons per unit time emitted into 4π sterradians by the neutron source.
   A = area presented by the counter to the incident neutrons.
   d = distance from the counter face to the source.
   e = distance from the counter face to the effective centre of the Long Counter.
   D = d + e
   ε = the probability of obtaining a count when a neutron enters the solid angle of the counter.
   Eff = $A\varepsilon$ = efficiency of the Long Counter in terms of counts per unit neutron flux at the effective centre.

This can be rearranged to give the efficiency explicitly

$$Eff = \frac{C \ 4\pi D^2}{n}$$

or in terms of the slope S of the inverse square plot, where

$$S = \frac{1}{D\sqrt{C}}$$

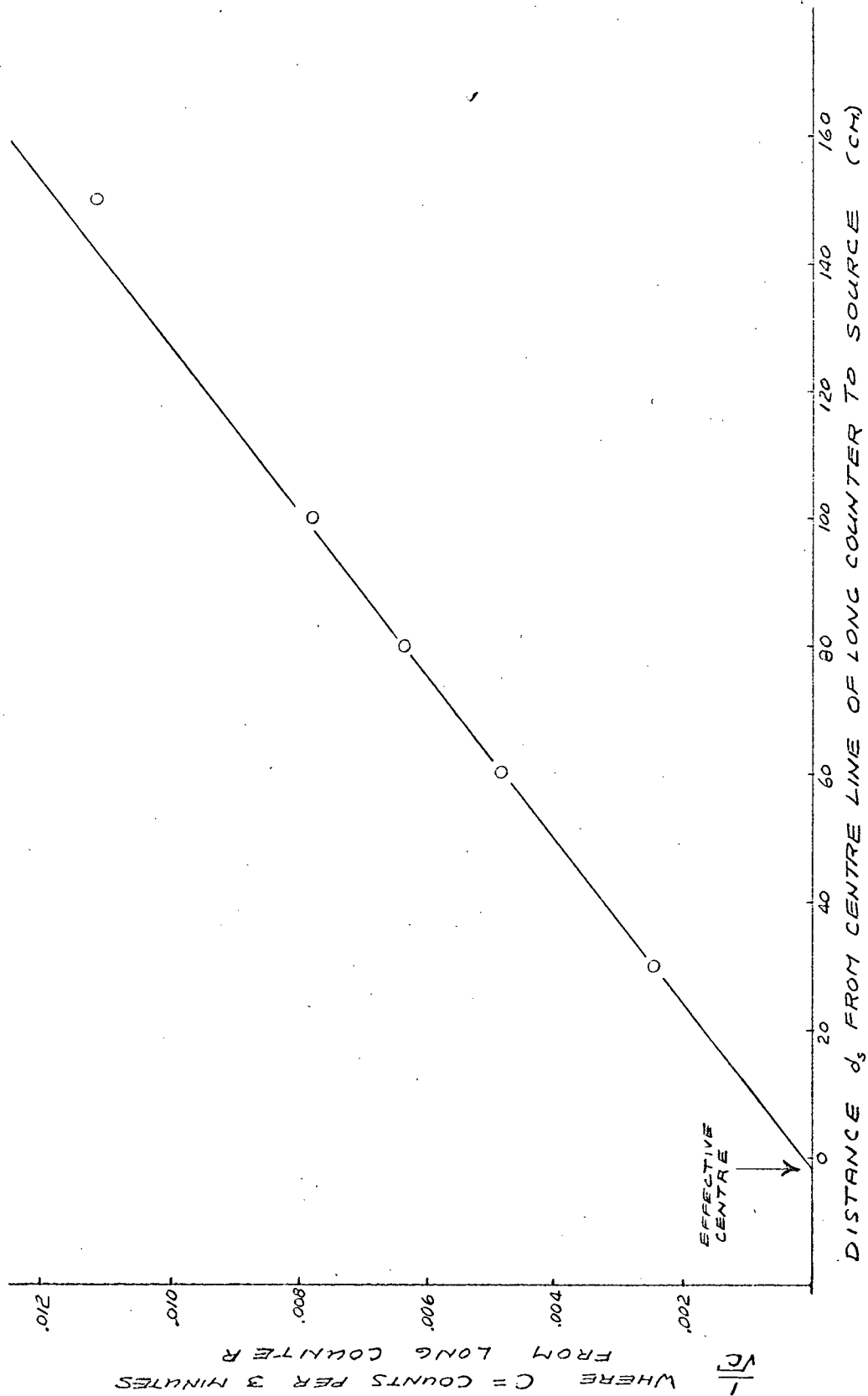FIGURE 7. INVERSE SQUARE PLOT FOR AmBe NEUTRONS COMING
FROM SIDE OF LONG COUNTER.

DISTANCE d_s FROM CENTRE LINE OF LONG COUNTER TO SOURCE (CM)

$\frac{1}{\sqrt{C}}$ WHERE C = COUNTS PER 3 MINUTES FROM LONG COUNTER

the efficiency can be expressed as $Eff = \frac{4\pi}{nS^2}$.

The slope S of Fig. 6 for $d \leqslant 100$ cm was found to be 2.549 x 10^5 ($\pm$ 0.1%). This combined with the neutron source strength of 7.62 x 10^5 ($\pm$2%) neutrons per second, gives an effeciency

$$Eff = 14.1 \ (\ \pm2.2\% \ ) \ \text{counts per neutron per } cm^2$$
at the effective centre

Using the same slope, the effective centre was found to be at e = 10.8 ($\pm$5.5%) cm behind the front reference face of the counter shown in Fig. 3.

The efficiency can also be stated in terms of the fraction of neutrons emitted by a source which produce counts in the counter. This clearly depends on the distance of the source from the counter. The present counter can be compared with the counter in its original form in terms of the relateve number of counts obtained when the source was placed at 150 cm from the face. The original U.B.C. Long Counter contained a 1 inch diameter BF_3 counter as described on page 2. Using a RaBe neutron source at 150 cm this counter gave 4.6 x 10^{-6} counts per neutron emitted by the source (Heiberg, 1954). For an AmBe source of approximately the same strength, at the same distance, the new counter gave 4.74 x 10^{-5} counts per neutron emitted by the source, more than an order of magnitude improvement.

Results for the source at the side of the counter are shown in Fig. 7 where the inverse square root of the counting rate is plotted against the distance d_s from the counter centre line to the source.

The slope of this plot for $d_s \leq 100$ cm was found to be $7.74 \times 10^{-5} \pm 1.6\%$. Using this slope and the method described previously (page 10), the Long Counter efficiency for neutrons incident from the side was calculated to be $15.3 \pm 5.2\%$ counts per unit neutron flux at the effective centre. The effective centre in this case was obtained by extrapolation of the plot in Fig. 7 to the distance axis, and found to be 1.6 ($\pm 2\%$)cm behind the centre line of the counter.

The efficiency per unit flux for neutrons incident on the side is thus slightly larger than that previously calculated for the same flux incident on the end. However, since the cross sectional area of the sensitive region from the side, A_s, is 2.7 times that from the end, A_a, this implies a lower intrinsic efficiency ε for neutrons incident on the side. From the data we have for the end

$$(Eff)_a = A_a \, \varepsilon_a = 14.1$$

and for the side

$$(Eff)_s = A_s \, \varepsilon_s = 15.3$$

Therefore the ratio of the intrinsic efficiencies is

$$\frac{\varepsilon_s}{\varepsilon_a} = \frac{15.3}{14.1} \frac{A_a}{A_s} = \frac{15.3}{14.1} \times \frac{1}{2.7} = 0.402$$

This indicates that the shielding on the Long Counter reduces the intrinsic efficiency for neutrons incident from the side compared to the efficiency for those entering the front end. This reduces the effect of background and room scattered neutrons.

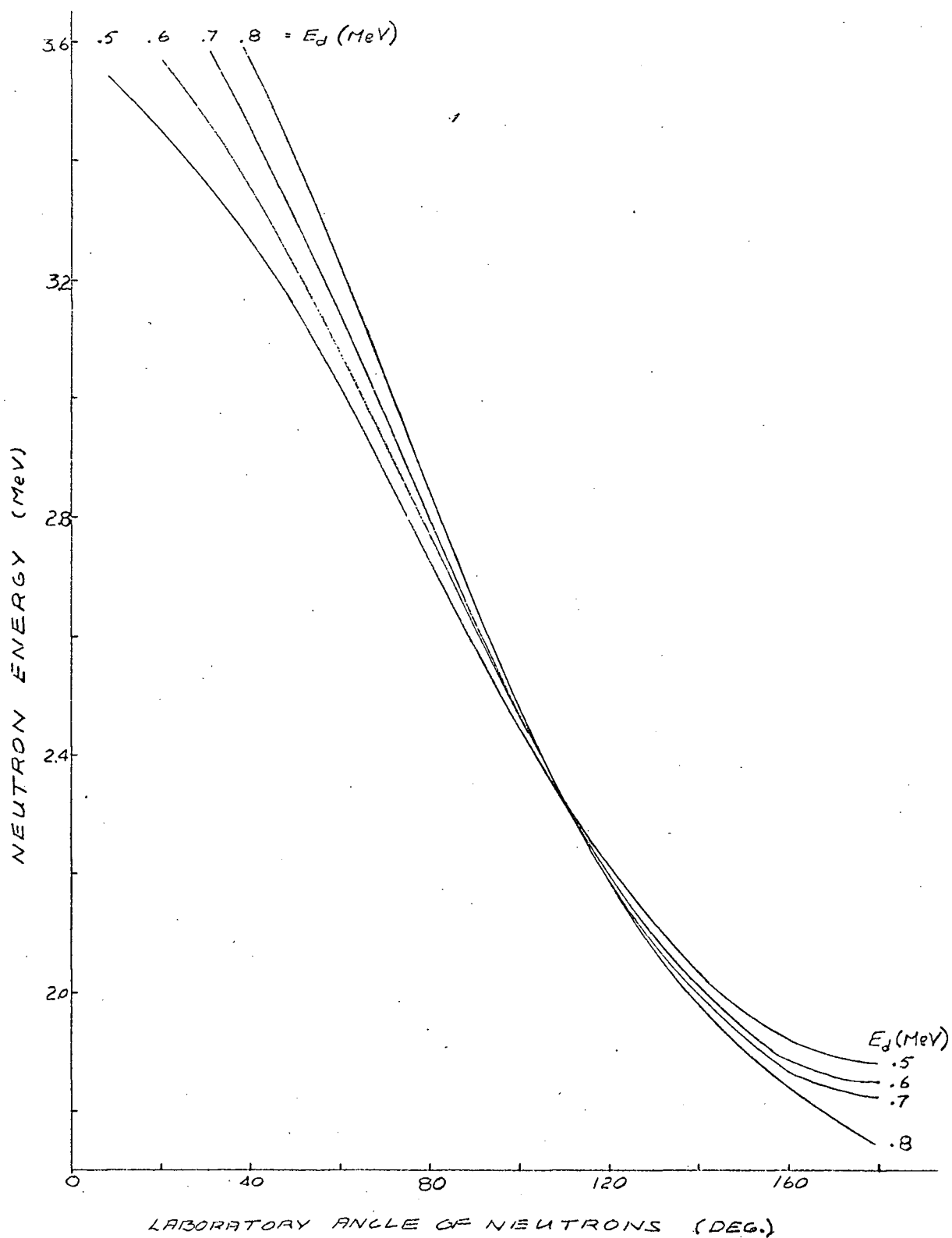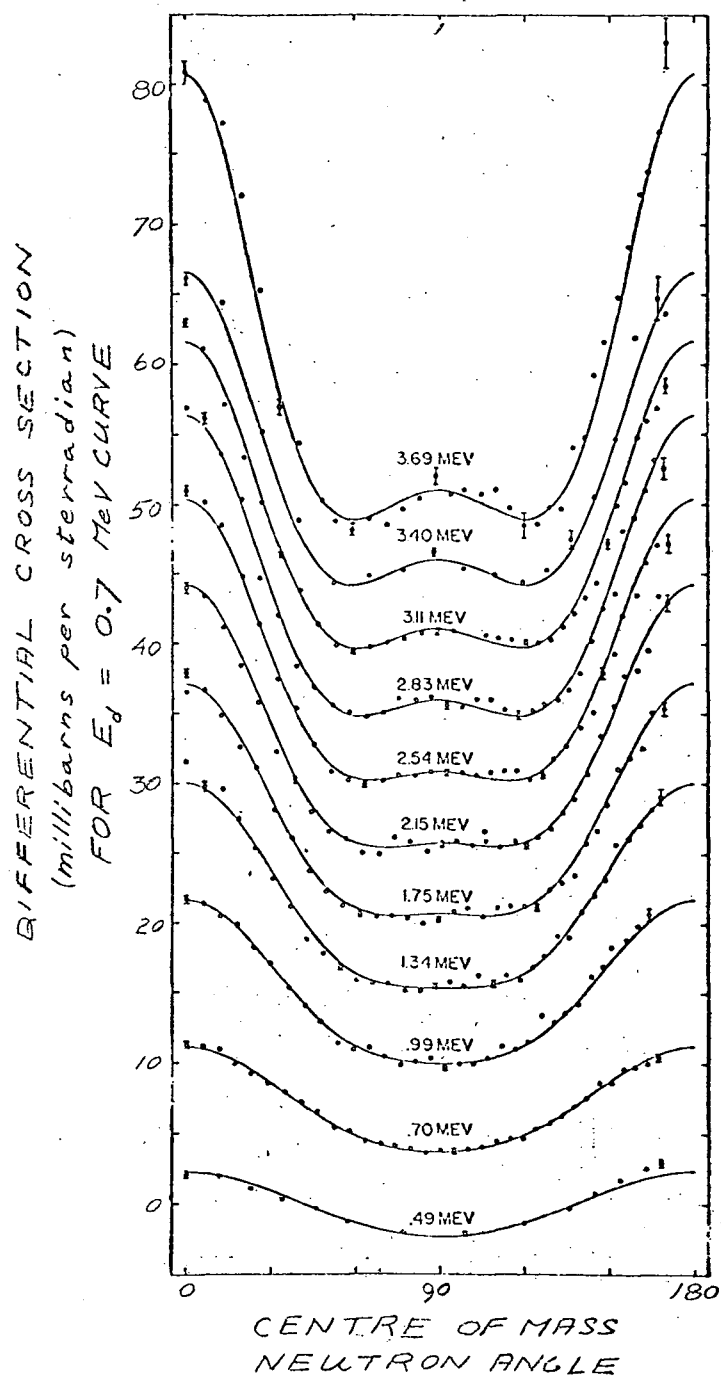FIGURE 8. $D(d,n)^3He$ NEUTRON ENERGY VERSUS LABORATORY ANGLE OF NEUTRONS FOR VARIOUS DEUTERON ENERGIES (FOWLER AND BROLLEY 1956)

FIGURE 9.   D(d,n)³He DIFFERENTIAL CROSS SECTION VERSUS CENTER OF MASS NEUTRON ANGLE FOR SEVERAL DEUTERON ENERGIES. THE 0.4 MeV CURVE HAS BEEN SHIFTED DOWN BY 5 mb/st, AND EACH OF THE CURVES $E_d \geqslant 0.99$ MeV HAS BEEN SHIFTED UP BY 5 mb/st FROM THE PRECEEDING ONE TO PREVENT OVERLAPPING.

CHAPTER III

MEASUREMENT OF LONG COUNTER EFFICIENCY

USING THE REACTION $D(d,n)^3He$

3.1. The Reaction $D(d,n)^3He$

At low energies, collisions between two deuterons result in the

two reactions $D(d,n)^3He$ and $D(d,p)T$ with approximately equal probability

and Q-values of 3.268 MeV and 4.033 MeV respectively. If the input

energy of the reaction is increased, a tertiary process, involving the

breakup of the deuteron, occurrs with a Q-value of -2.225 MeV.

Fig. 8 shows the variation in neutron energy with the neutron

angle and incident deuteron energy for the reaction $D(d,n)^3He$ (Fowler and

Brolley, 1956).

Fig. 9 shows the differential cross section for the reaction

$D(d,n)^3He$ for various incident deuteron energies as a function of the

centre of mass angle. The data shown were obtained by Hunter and

Richards (1949) using a calibrated Hanson-McKibben Long Counter to detect

the neutrons produced in a gas target 2 cm in length. The neutrons were

observed rather than the ^3He in order that measurements could include all

angles in centre of mass from 0° to nearly 180°. Background neutrons

from the foil and collimating apertures amounted to only 2% of the

$D(d,n)^3He$ yield at a deuteron energy of 0.7 MeV. The data shown in Fig. 9

have been corrected for the variation of Long Counter efficiency with

neutron energy using the curve given in McKibben (1947) and converted to

SCALE   INCHES

0   1   2   3   4   5

BEAM

VIEWING WINDOW

TANTALUM COLLIMATORS 0.1" APERTURE

REMOVABLE COPPER-QUARTZ BEAM STOP

LUCITE

GAS INLET

COPPER - CONSTANTAN THERMOCOUPLE

GLASS TUBE

BACKSTOP

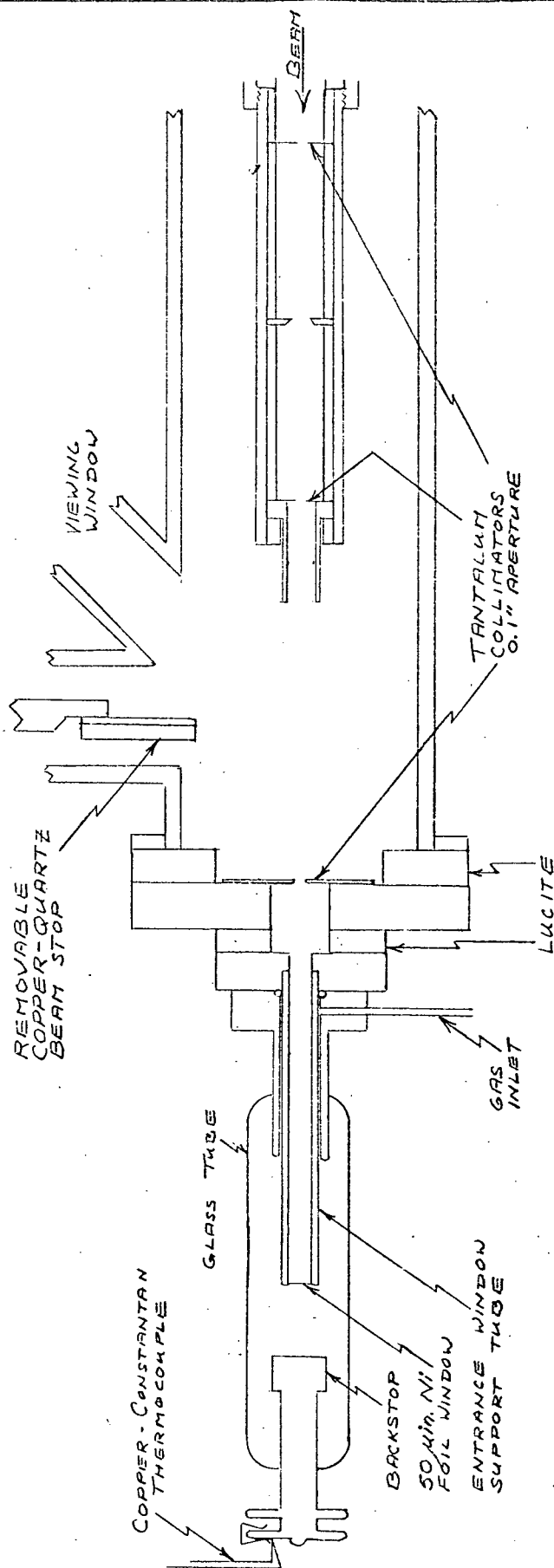50 μin. Ni FOIL WINDOW

ENTRANCE WINDOW SUPPORT TUBE

FIGURE 10. GAS TARGET AND COLLIMATION SYSTEM

centre of mass. The appearance in the data of the symmetry of the differential cross section about 90° in the centre of mass system as required by the identity of the initial particles, verifies the applicability of McKibben's curve to the Long Counter used.

The statistical errors in the data were $\leq \pm 5\%$ and the Long Counter calibration was accurate to $\pm 5\%$ giving a total error on the cross sections of 10%.

3.2.   The Gas Target

The gas target system used is illustrated in Fig. 10.

The Nickel Foil Entrance Window

Manufacturer: Chromium Corporation of America, Waterbury, Conn.,U.S.A.

Specifications: Grade C, Dimensions $\frac{1}{2}$" x $\frac{1}{2}$" x 50μ inches

The foil thickness was determined for $\simeq$0.9 MeV protons by investigating the shift in the 0.873 MeV gamma resonance from proton bombardment of fluorine. Sufficient fluorine contamination was present on the gas target backstop and on the metal backing of a beamstop in the beamline before the collimators to make actual deposition of a fluorine target unnecessary. The fluorine gamma peak before the window was centered about 876 ± 2 keV with a half-width of 7 keV, and that after the window , at 1015 ± 4 keV with half width 12 keV, indicating a window thickness of 139 ± 6 keV for $\simeq$0.9 MeV protons.

The foil was soldered over the end of the brass support tube using "Stay-Brite" solder. The end of the tube was dipped in a puddle of molten solder and flux on an aluminum plate so as to retain a small

amount of solder on the end. The tube was then clamped solder end up, a nickel foil laid across the end and a small aluminum block set on the foil. The block was then heated, melting the solder. Foils attached in this manner were found to withstand pressure differences of $\simeq 740$ mm Hg, the lower pressure being inside the support tube, before rupturing. Using an electrical contact system, a pressure difference of 300 mm Hg was found to cause a depression in the foil of 0.012 cm from the position of the foil with equal pressures on both sides. This represents a 1.4% change in the 0.833 cm length of the beam path in the gas cell.

Target Thickness

The purpose in using a gas target was the ease of determination of the number of target nuclei, which can be calculated using the path length in the gas from the entrance foil to the backstop, the gas pressure in the target, and the temperature in the beam region of the gas.

The pressure of the target gas was measured using a 0 to 800 mmHg Wallace and Tiernan absolute pressure meter, and the target region length was measured with a travelling telescope.

Because of the power dissipated by the incident deuteron beam, the temperature in the beam region is generally slightly greater than that in the bulk of the gas in the target. The extent of this effect has been measured and plotted for various beam currents by Robertson et al (1961) using the same gas target being used in the present experiment. Due to the large copper backstop, it was assumed that the temperatures of the bulk of the gas in the target and that of the backstop would be

essentially the same. This temperature was measured using a copper-constantan thermocouple affixed to the backstop. The effective temperature in the beam region is described in terms of the temperature T of the bulk of the gas as

$$T_{eff} = (P_i / P_o) T$$

where (P_i/P_o) is given by Robertson's plot as

Beam Current	(P_i/P_o)
.02 µamp	1.001
.1	1.005
.2	1.012

3.3. Current Integration

Even at very low beam currents the target gas will experience considerable ion zation. This was confirmed by the fact that a distinct blue glow was seen in the beam region in the gas, which in fact was used to check the centering of the beam in the foil window support tube. The slightest potential difference between the window and backstop portions of the target would cause charge separation, making current measurements from the backstop completely unreliable.

The only way to eliminate errors in the current measurement resulting from charge separation in the gas, or from preferential collection of secondary electron emission, was to connect the window and backstop portions electrically and measure the total current entering and stopped in the gas cell. This method, however, presents the problem that if some of the deuteron beam is lost on the sides of the tube holding the window, positive current is measured which does not actually
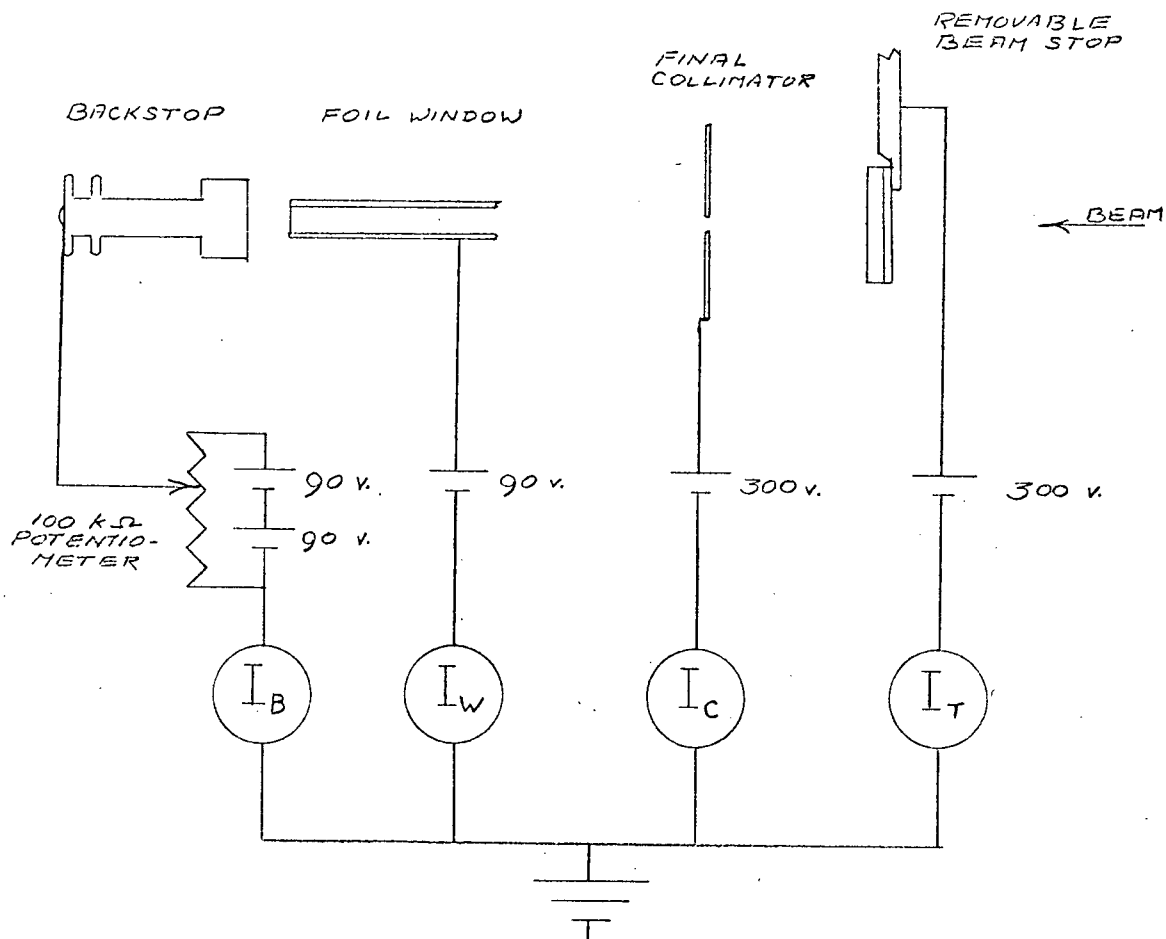
FIGURE 11. CURRENT MEASUREMENT AND VARIABLE BIAS ARRANGEMENT FOR CURRENT DISTRIBUTION INVESTIGATION.

pass through the target gas.

To prevent any current falling on the tube supporting the foil at the entrance to the gas cell, the beam collimation system was designed such that a particle passing through the collimators at even the most extreme angle would pass through the window into the gas without hitting the walls of the entrance tube. Also, the focussing was arranged to give as nearly as possible a parallel beam and rule out any chance of a focus inside the collimation system.

These precautions were shown to be effective in a current distribution check using the apparatus described in Fig. 11. The final collimator was held at +300 v in order to retain any electrons knocked out of it by the incident beam. The window portion was held at +90 v so that the potential difference between it and the backstop could be varied from +90 v to -90 v continuously. Using this arrangement an investigation was made, with no gas in the target, of the currents on different parts of the target chamber and collimation system, resulting from both a proton beam directly and the secondary electron emission.

The total current was measured, with a +300 v bias, on a removable metal beam stop just in front of the final collimator. Then, with the beam stop removed, simultaneous currents were measured on the final collimator, the foil window and its supporting tube, and on the backstop, as shown in Fig. 11, for various relative potentials on the foil window and backstop.

To 10% the net current agreed with the total current measured on the removable stop, indicating that no beam was being lost other than

on the three parts considered. This agreement at the point where the window current is zero further indicates that all current that goes through the collimator, passes through the foil window and the gas cell and hits the backstop with none being lost on the sides of the entrance tube.

The high saturation currents at negative backstop bias, indicate a higher rate of secondary electron emission from the backstop than from the foil window.

The total charge entering and stopped in the gas cell was measured on the connected window and backstop using an Eldorado Electronics model CI-110 current integrator (Eldorado Electronics, Berkeley, Calif.). The trip-meter pointer was set to full scale before the runs with the Long Counter were begun and was left unchanged until all runs and the current integrator calibration check had been completed.

The current integrator calibration on the range used during the runs was checked using a 1.01902 (±0.01%) volt standard cell, and an accurately measured 5.0116 (±0.005%) ohm resistor. These gave an input current of 0.20303 µa which was measured by the current integrator for 52' 4", or 14 cycles of 45 µcoulombs each. Comparison of the input charge and the charge integrated indicated the current integrator to read within 1.25%.
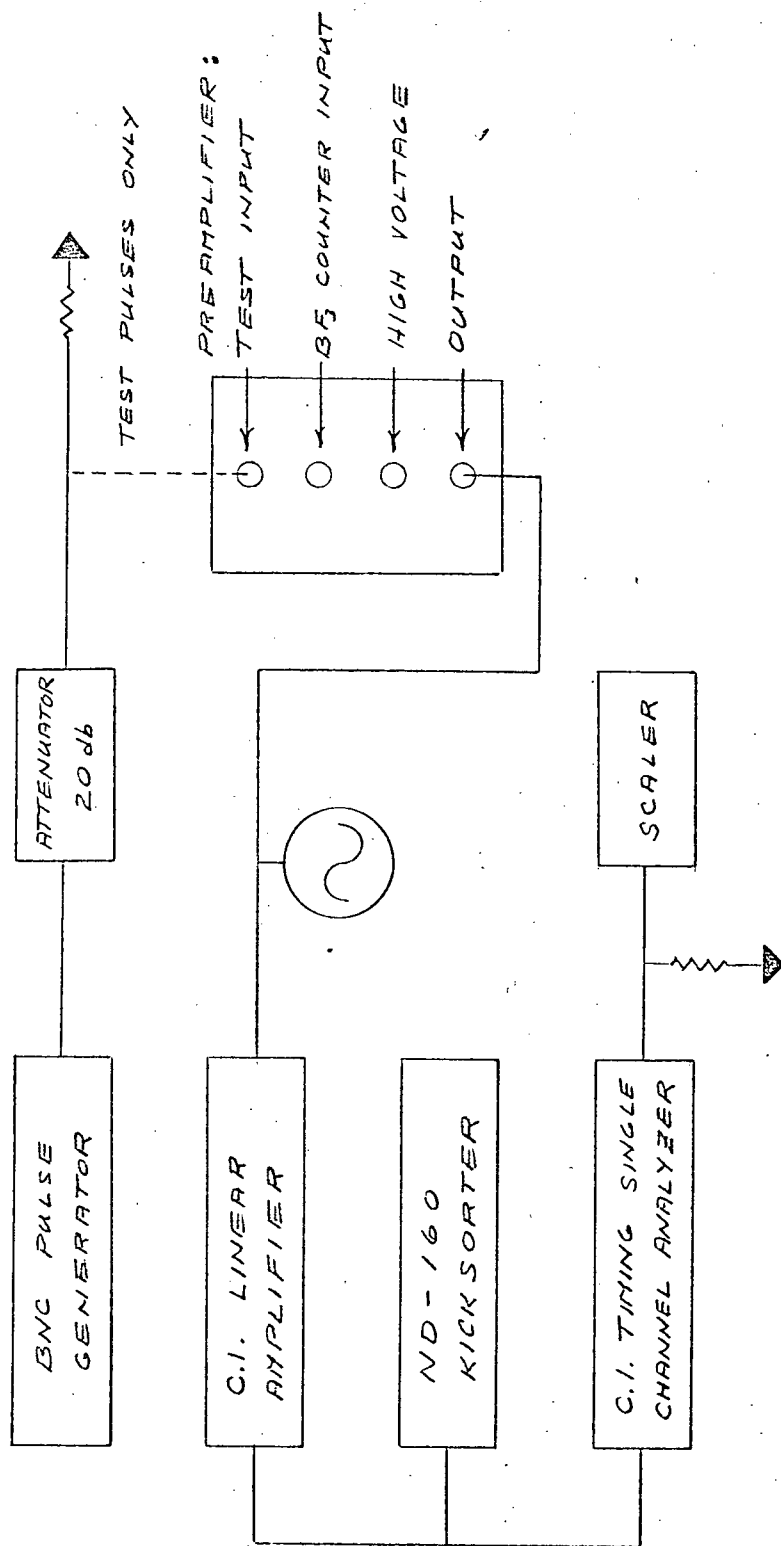
FIGURE 13. ELECTRONICS FOR LONG COUNTER CALIBRATION USING THE REACTION D(d,n)^{3}He. RECOMMENDED FOR GENERAL USE OF THE LONG COUNTER.

3.4. Measurements

The experimental arrangement was that shown in Fig. 3 (page 7), the neutron source in this case being the gas target.

The pulses from the BF_3 tube were amplified and analyzed as shown in Fig. 13. The linearity of the kicksorter was checked, and the window limits of the single channel analyzer were set using a pulse generator which was able to produce pulses very similar to those from the BF_3 tube. These test pulses were injected with a 51 Ω termination at the preamplifier test input.

Using a 776 keV deuteron beam of 250±20 nanoamps at the gas cell from the U.B.C. Van de Graaff generator, a series of 44 runs were made, each having a total collected charge of 45 μcoul. or 90 μcoul., an even one or two cycles of the current integrator. For each run the Long Counter was placed at a distance between 30 cm and 200 cm, measured from the front face of the centre paraffin region to the centre of the gas cell, and along one of two lines drawn at 60° and 90° to the direction of the incident deuteron beam in the gas cell. The gas target was filled with 200 torr of either deuterium or hydrogen, the latter for background runs.

Table 3 gives an outline of the run schedule.

TABLE 3

Run Schedule

Run	Long Counter Direction	Target Gas
1 - 8	90°	H_2
9 - 15	90°	D_2
16 - 22	90°	H_2
23 - 25	60°	H_2
26 - 32	90°	D_2
33 - 37	60°	D_2
38 - 41	90°	H_2
42 - 44	60°	H_2

The resulting spectra were punched on paper tape directly from the kick sorter memory and later converted to cards by the U.B.C. computing centre for use with a neutron peak integrating program. All spectra had the same characteristic shape shown in Fig. 4. A short computer program was used to integrate all the spectra, with the bias set as shown in Fig. 4, and the accumulated running time at the beginning of each run. A beam-off run was made to determine the time dependent room background. All counts were corrected for kicksorter dead time, which only twice exceeded 4%, and for time dependent background, which never exceeded 3% of the total count rate and was almost always considerably less than 3%.

3.5. Background

The accumulated time was used as a clock to study the background increase with time due to neutrons from deuterium build-up on the collimators and backstop. The neutron counts remaining in the H_2 runs
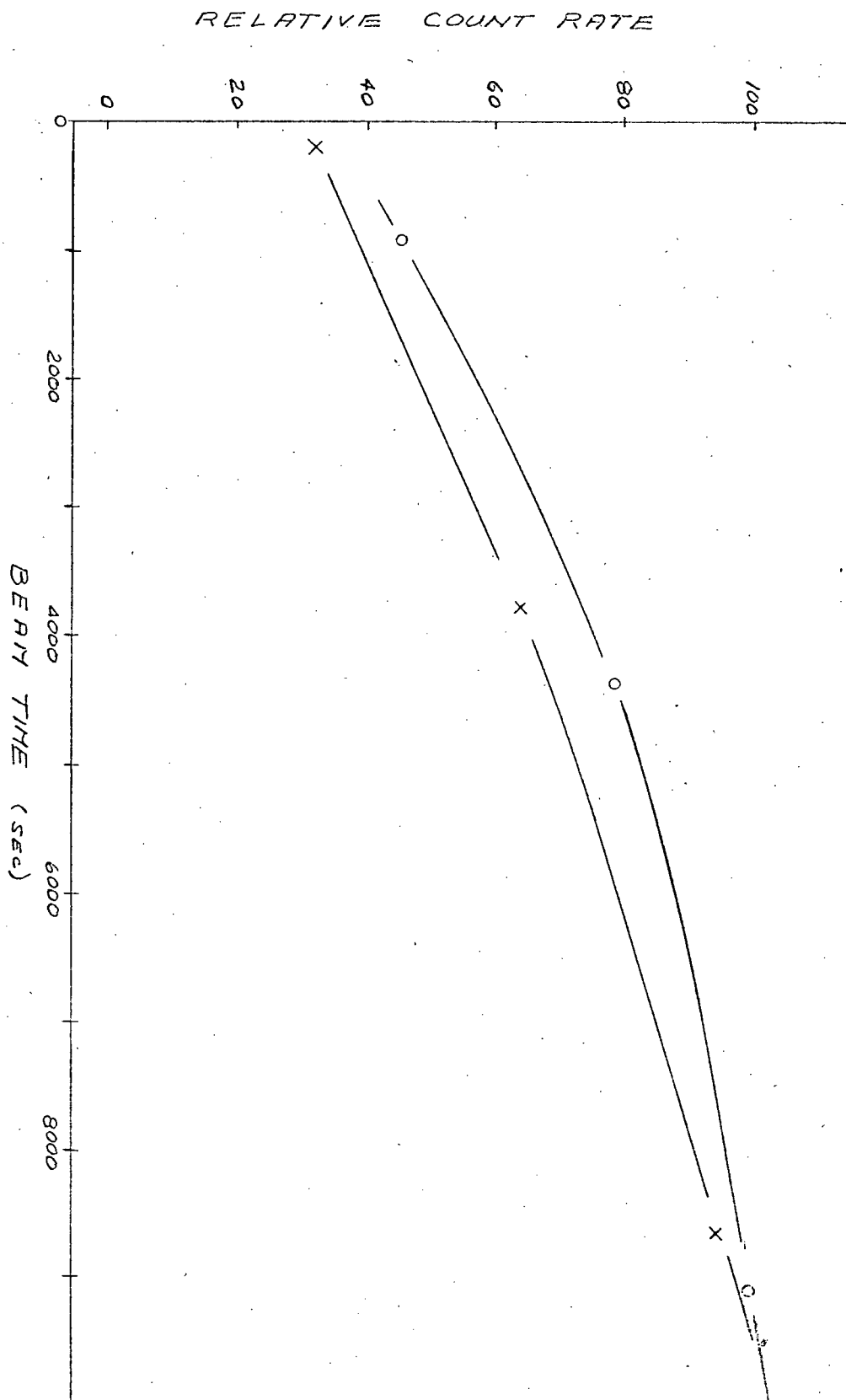
FIGURE 14. INCREASE OF BEAM DEPENDENT BACKGROUND WITH RUNNING TIME.

after subtraction of the time dependent background represented the
background due to deuterium contamination in the target chamber and
collimation system. These count rates were plotted against the 'clock'
time of the midway point of the run, to produce a family of curves
showing the background buildup with beam-on time at Long Counter
distances of 30 cm, 50 cm, 75 cm, 100 cm, 130 cm, 150 cm, and 200 cm at
90°; and 35 cm, 75 cm, and 130 cm at 60°. Two of these curves were
normalized to produce Fig. 14. It can be seen that even after almost
3 hours with actual beam on target, or 2385 µcoulombs of deuterium
stopped in the gas cell, the neutron yield due to build-up of deuterium
on the surfaces shows no tendency to level·off as would result from
saturation of the surfaces. The greatest portion of this background
will be from the backstop where most of the beam is stopped. The
failure to saturate is in agreement with a calculation based on a
discussion by J.H. Coon in Marion and Fowler (1960), which indicates
that for the beam current and configuration, and the gold backstop
used in this experiment, a total charge of about 4200 µcoulombs would
be collected by the backstop before saturation became significant.
The original curves for individual distances were used to read off the
background seen by the Long Counter at a particular distance, angle and
time. These backgrounds were then subtracted from the D_2 runs to
determine the count rate due to the target gas alone. To determine
the beam dependent background for runs at Long Counter distances where
no background data was taken, such as 100 cm at 90°, plots were made

of $B(d,t)^{-\frac{1}{2}}$, where $B(d,t)$ is the background count rate at distance d

and at t, the mid-time of the run in question, versus the distance d.

Interpolation then gave the background at the desired distances.

3.6. Gas Target Thickness

The thickness of gas traversed by the deuteron beam is defined by

the pressure and temperature of the gas in the beam region, and the

geometrical distance between the entrance window and the backstop.

The gas cell length was measured, using a travelling telescope,

to be 0.833 (±0.3%) cm. Thus, including the foil depression, the

beam path length was 0.845 (±0.5%) cm.

The gas pressure for all runs was 200 torr (±2%). Any difference

between the meter pressure and the gas pressure in the beam region was

corrected for by the effective temperature correction.

The temperatures measured on the backstop cooling fin varied by

± 0.24% about an average of 295.2°K. For the current range

250 ± 20 nanoamps used in the runs, the temperature correction factor

for gas heating in the beam region is 1.001 (±0.1%) (Robertson et

al, 1961). This gives an effective temperature in the beam region of

295.5 (±0.34%) °K.

Using these parameters, N_t, the number of target nuclei per square

centimeter in the gas cell was:

$$N_t = \frac{2N_o}{V_o} \times L \times \frac{P}{P_o} \times \frac{T_o}{T} = 1.11 \times 10^{19} \ (\ \pm 2.8\% \ )$$

$$\text{target nuclei} \ / \ cm^2$$

where: N_O = Avagadro's number.
         V_O = Volume of one mole of gas at STP.
         L   = Length of beam path in gas cell.
         P   = Gas pressure.
         P_O = 760 torr.
         T_O = 273°K
         T   = Effective temperature in beam region.

3.7.   Beam Energy in the Gas Cell

A check of the Van de Graaff energy calibration indicated that the meter read 3 keV high, so that the meter energy reading of 776 keV used during the runs indicated a beam energy of 773 (±0.4%) keV entering the foil window. The foil window thickness was 138 (±2.3%) keV for 900 keV protons, which corresponds to a thickness of 228 (±3.6%) keV for 773 keV deuterons (page 683, Marion and Fowler, 1960). Thus the deuteron beam entered the gas cell with an energy of 545 (±2.0%) keV. Deuterons of this energy are slowed in deuteriom gas at the rate of 3.1×10^{-15} ev per gas atom per cm^2 (page 681, Marion and Fowler, 1960). Thus the approximate energy of the deuteron beam midway across the gas cell would be 528 (±2.1%) keV. Recalculating, using this approximate energy in the gas to determine a better average energy loss rate, the beam energy midway through the gas was found to be 527 (±2.1%) keV.

3.8.   Neutron Flux from the Gas Target

The number of neutrons emitted from the target in the direction of the Long Counter can be calculated using the reaction cross section for the appropriate angle and deuteron beam energy, the thickness of gas in the gas cell, and the number of deuterons incident on the target

gas. The average beam energy in the gas cell was found in section 3.7 to be 527 (±2.1%) keV. Interpolating to this energy using the curves of Fig. 9, the differential cross sections for the reaction $D(d,n)^3He$ at 60° and 90° in the laboratory system were found to be 3.18 (±10%) millibarns per sterradian and 3.03 (±10%) millibarns per sterradian, respectively. The gas target thickness was found in section 3.6 to be 1.11×10^{19} (±2.8%) target nuclei per cm^2. The charge collected during each cycle of the current integrator was found, on page 18, to be 45 (±1.25%) μcoulombs. Thus, during each cycle, the number of deuterons entering the gas cell was

$$N_d = \frac{45 \; \mu coul}{1.6 \times 10^{-13} \; \mu coul./ deuteron}$$

$$= 2.81 \times 10^{14} \; (\pm 1.25\%) \; deuterons$$

The differential cross section at angle θ is defined as

$$\sigma_\theta = \frac{N_n}{N_d \times N_t}$$

where: N_n = Number of neutrons per sterradian emitted per integrator
          cycle at angle θ.
        N_d = Number of deuterons incident on the target per cycle.
        N_t = Number of target nuclei per cm^2.

Thus $N_n = \sigma_\theta N_d N_t$. In order to use the method described in section 2.3 to calculate the efficiency, the number of neutrons emitted by the reaction must be expressed as the number of neutrons emitted into 4π sterradians by an isotropic source. In spite of the finite solid angle subtended at the gas cell by the Long Counter, it was found that the neutron energy and cross section varied little across the sensitive
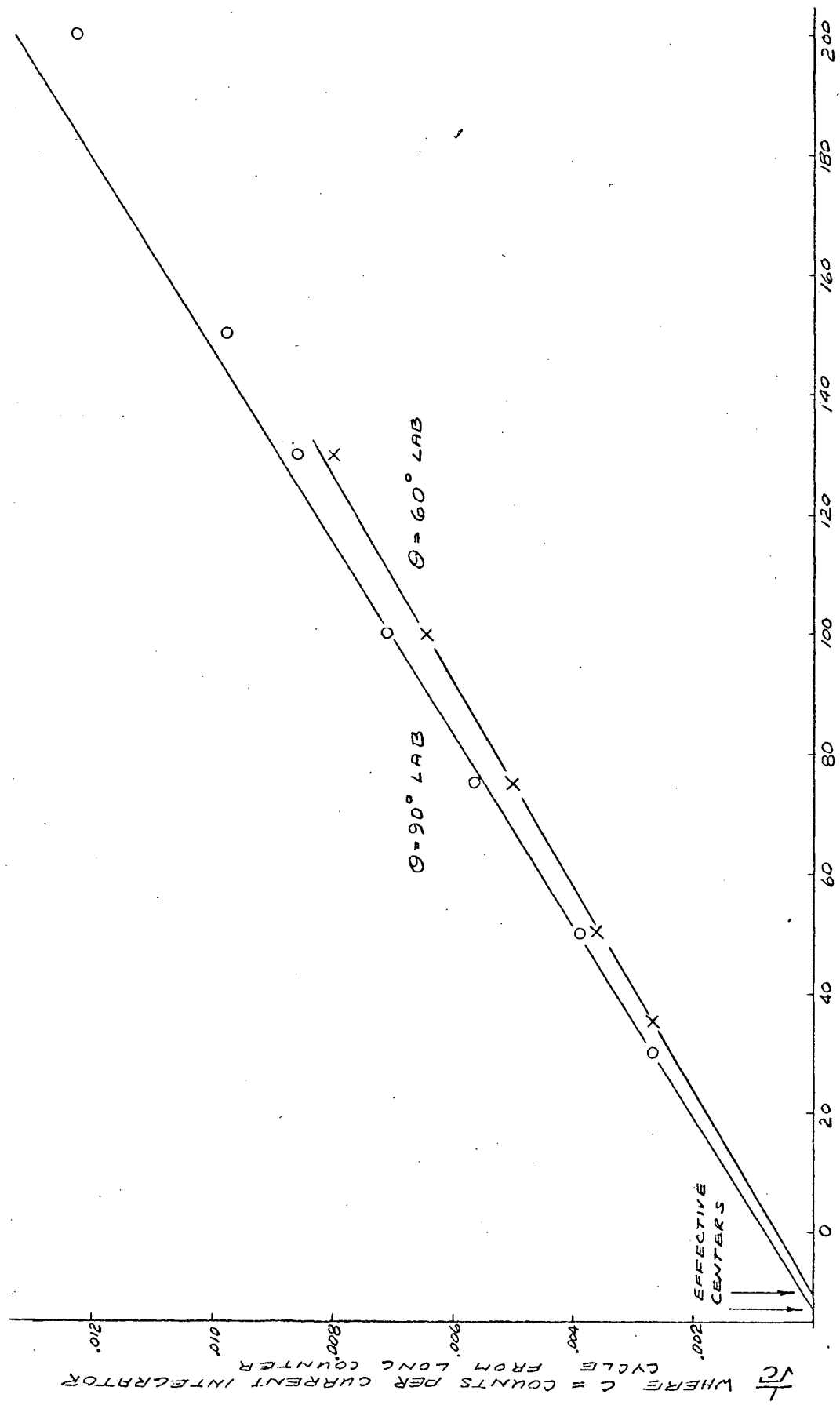
region, so that no correction was necessary for the spread in angles due to the finite size of the detector at 60° and 90°. The reaction was therefore sufficiently isotropic over the range of angles included by the counter at either 60° or 90° that n in the effeciency calculation on page 10 could be expressed as

$$n_{\theta} = 4\pi \ N_n = 4\pi \ \sigma_{\theta} \ N_d \ N_t$$

Therefore $n^{*}_{60} = 1.25 \times 10^{8}$ ($\pm14\%$) neutrons per integrator cycle emitted in all directions

and $n_{90} = 1.19 \times 10^{8}$ ($\pm14\%$) neutrons per integrator cycle emitted in all directions.

Due to the geometry of the gas cell, at angles different from 90° the counter face will be partially shadowed by the backstop. When the Long Counter is at 60° to the direction of the deuteron beam in the gas cell, 32.7% of the beam path length is shadowed by the backstop. The neutrons emitted in the direction of the Long Counter by this shadowed portion of the beam pass through an average of 0.276 cm of copper in the backstop. The total cross section for neutrons in copper is 4 barns (Hughes and Schwartz, 1958), so that 9.2% of the neutrons entering the backstop will be lost. Combining these fractions, it is estimated that at 60°, 3.01% of all the neutrons emitted into the solid angle of the Long Counter will be lost in the backstop. Applying this correction to n^{*}_{60} gives $n_{60} = 1.21 \times 10^{8}$ ($\pm14\%$) neutrons per integrator cycle, emitted in all directions.

FIGURE 15. INVERSE SQUARE PLOT FOR LONG COUNTER CALIBRATION USING THE REACTION $D(d,n)^3He$.

DISTANCE FROM LONG COUNTER FACE TO GAS CELL (cm.)

$\frac{1}{\sqrt{C}}$ WHERE C = COUNTS PER CURRENT INTEGRATOR CYCLE FROM LONG COUNTER

$\theta = 60°$ LAB

$\theta = 90°$ LAB

EFFECTIVE CENTERS

3.9. Calculation of Efficiency

Following the procedure used in section 2.3 for the AmBe calibration, a plot was made of $C^{-\frac{1}{2}}$ against the distance from the counter face to the centre of the gas cell, where C is the number of counts per integrator cycle from the Long Counter. The slope of this plot, shown in Fig. 15, was found to be $S_{60} = 5.94 \times 10^{-5}$ (±2.4%) for the Long Counter at 60°, and $S_{90} = 6.3 \times 10^{-5}$ (±2.8%) for the counter at 90°, and the corresponding effective centres were found to be at -10.3 (±7%) cm and -12.6 (±9%) cm, respectively. Both slopes represent the region d≤100 cm, as the room scattered neutron background becomes significant beyond that point, as indicated by the deviation of the data from the inverse square law. The efficiency was then calculated as

$$\text{Eff}_{\theta} = \frac{4\pi}{n_{\theta} S_{\theta}^2}$$

where n_{θ} is the number of neutrons emitted by the reaction in all directions, assuming isotropy. It was found in section 3.8 that

$$n_{60} = 1.21 \times 10^8 \ (\pm 14\%) \text{ neutrons per cycle into } 4\pi$$
$$\text{assuming isotropy}$$

and

$$n_{90} = 1.19 \times 10^8 \ (\pm 14\%) \text{ neutrons per cycle into } 4\pi$$
$$\text{assuming isotropy}$$

so that

$$\text{Eff}_{60} = \frac{4\pi}{1.21 \times 10^8 \times (5.94)^2 \times 10^{-10}}$$

$$= 29.4 \ (\pm 19\%) \text{ counts per neutron per cm}^2 \text{ at the effective centre}$$

and

$$\text{Eff}_{90} = \frac{4\pi}{1.19 \times 10^8 \times (6.30)^2 \times 10^{-10}}$$

$$= 26.6 \ (\pm 20\%) \text{ counts per neutron per cm}^2 \text{ at the effective centre.}$$

The uncertainty on these efficiencies would be considerably reduced by more accurate measurement of the differential cross sections, which in this calculation accounted for 10% of the 19% or 20% uncertainty.
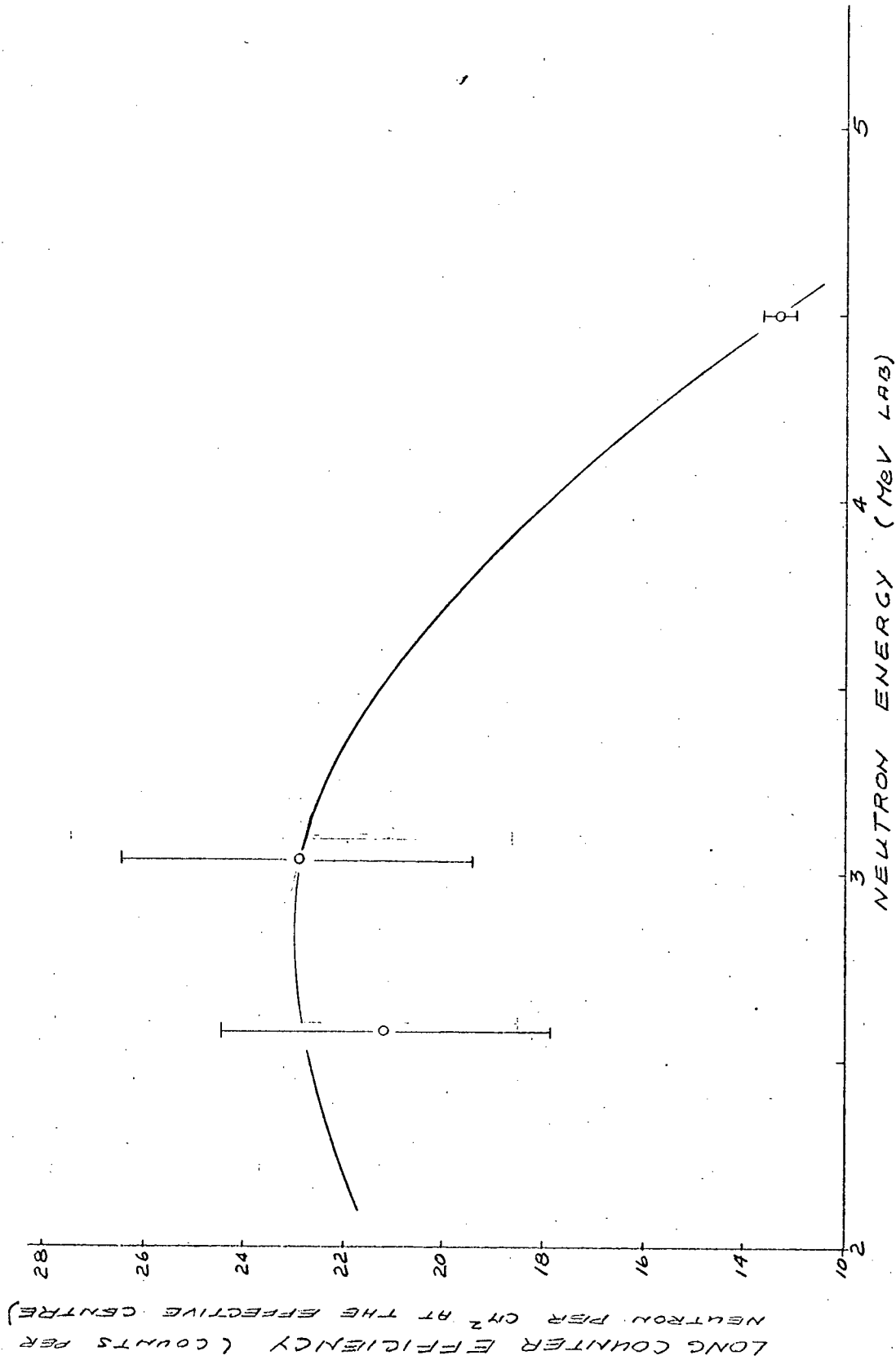
LONG COUNTER EFFICIENCY (COUNTS PER NEUTRON PER CM² AT THE EFFECTIVE CENTRE)

NEUTRON ENERGY (MeV LAB)

FIGURE 16. LONG COUNTER EFFICIENCY VERSUS NEUTRON ENERGY
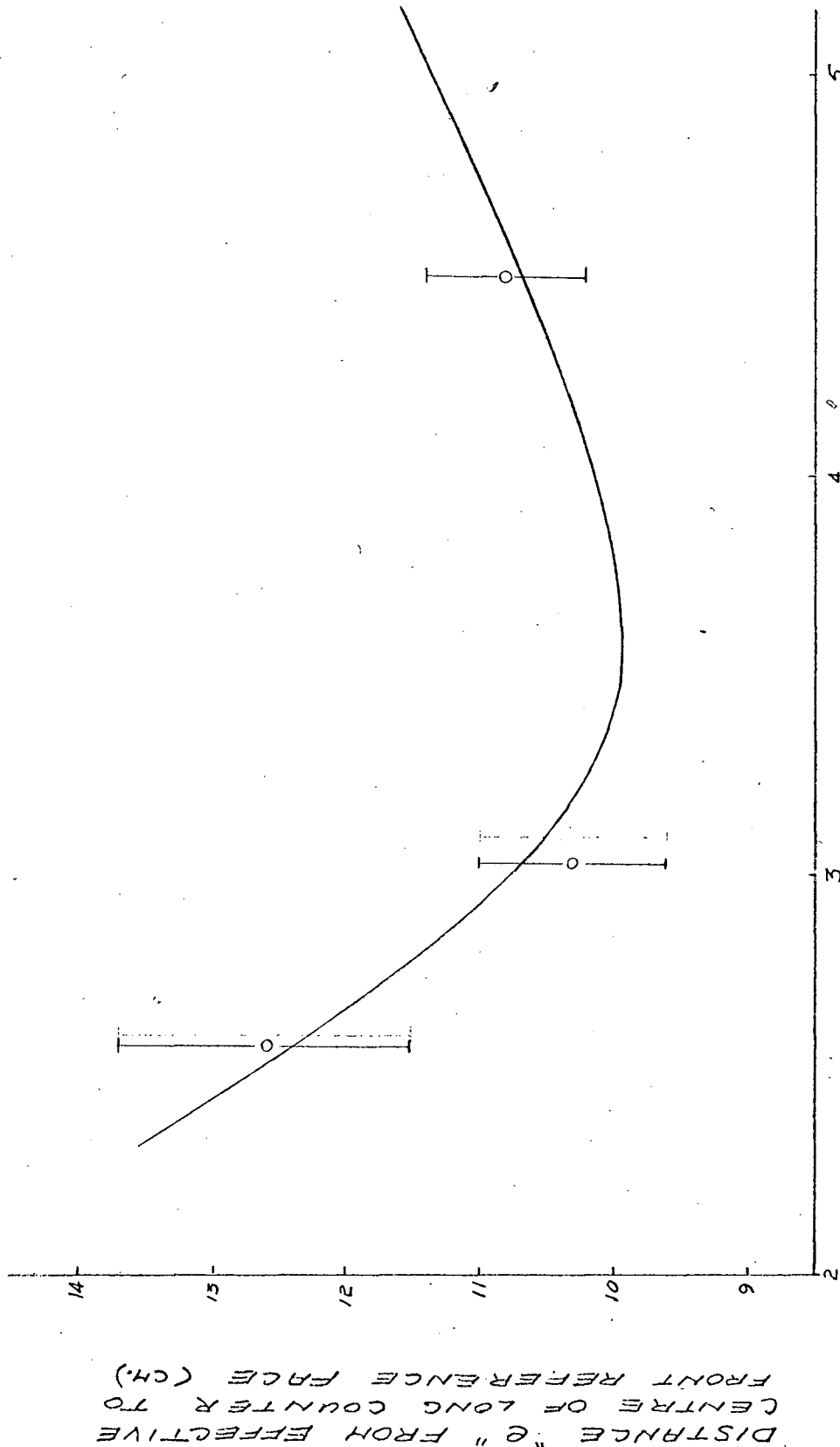
FIGURE 17. EFFECTIVE CENTRE OF LONG COUNTER
VERSUS NEUTRON ENERGY.

CHAPTER IV

CONCLUSIONS

In Fig. 16 the Long Counter efficiencies are plotted against neutron energy. The energy of the AmBe neutrons was determined from Fig. 2 to be approximately 4.5 MeV. The neutron energies produced at 60° and 90° by the reaction $D(d,n)^3He$ were interpolated from the data of Fowler and Brolley (1956) shown in Fig. 8, to be

Fig. 16 indicates considerable variation of the efficiency of the modified Long Counter with energy. This is due to the fact that the larger diameter BF_3 counter displaced a considerable amount of paraffin, thus reducing the amount of moderating material and leading to the loss of a higher proportion of high energy neutrons than with the smaller BF_3 counter. This reduction of paraffin would, on the other hand, allow a higher proportion of those neutrons that have been thermalized to reach the BF_3 tube and be counted. Fig. 17 shows the effective centre position plotted against neutron energy.

Thus for a gain of an order of magnitude in efficiency for high energy neutrons, and even more for low energy neutrons, one has sacrificed energy independence of the Long Counter. This is acceptable, however, as the neutron evergy spectrum is generally known in an experiment.

By modifying the original counter, the old calibration was
destroyed, but a factor of ten increase in efficiency was achieved
and the modified counter has been calibrated to better accuracy than
the original.

BIBLIOGRAPHY

Bramlett, R.L., R.I. Ewing, and T.W. Bonner, Nucl. Instr. Methods 9, 1(1960).

de Pangher, J., and L.L. Nichols, BNWL-260, Pacific Northwest Laboratory, Richland, Washington, 1966.

Fowler, J.L., and J.E. Brolley Jr., Rev. Mod. Phys. 28,112 (1956).

Geiger, K.W., and A.P. Baerg, Can. J. Phys. 43,373 (1965).

Hanson, A.O., and J.L. McKibben, Phys. Rev. 72,673 (1947)

Heiberg, S.A., Ph D Thesis, University of British Columbia, 1954.

Hornyak, W.F., Rev. Sci. Instr. 23,264 (1952).

Hughes, J.D., and R.B. Schwartz, Neutron Cross Sections, Brookhaven National Laboratory, Upton, New York, 1958.

Hunter, G.T., and H.T. Richards, Phys. Rev. 76, 1445 (1949).

Marion, J.B., and J.L. Fowler, Fast Neutron Physics Part I, Interscience Publishers Inc., New York, 1960.

Robertson, L.P., B.L. White, and K.L. Erdman, Rev. Sci. Instr. 32, 1405 (1961).

APPENDIX

LONG COUNTER ELECTRONICS

A.1. Proportional Counter

Reuter Stokes, Model # RSN 44A

|	
Filling Gas: BF_3 (96% ^{10}B)	Filling Pressure: 70 cm Hg
Outside Diameter: 2 1/32 "	Sensitive Length: 12"
Operating Voltage: +2200 v	Maximum Voltage: +3500 v
Max. Neutron Flux: 2.5×10^{13} n/cm^{2}sec	Maximum Temperature: 150°C
Res stance: $\geq 10^{12}\Omega$	Capacitance: 8 pf

A.2. Electronics for AmBe Calibration

D.C. Power Supply for Proportional Counter:

Hewlett-Packard, Harrison 6156A (Hewlett-Packard Co., Palo Alto, California)

Preamplifier Input:
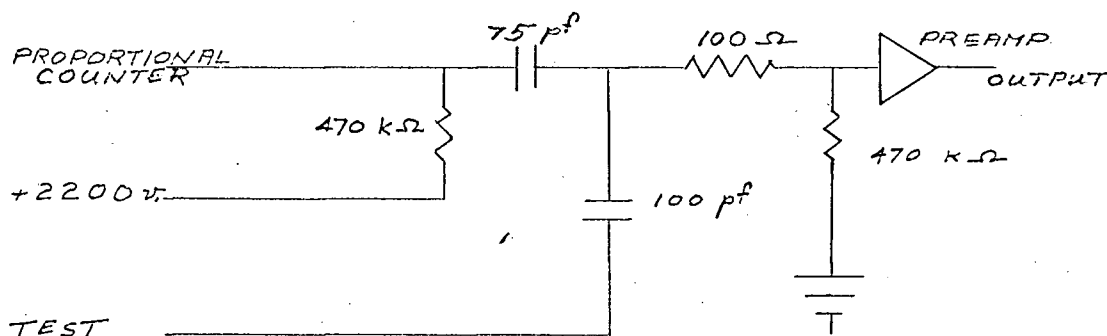
Preamplifier:

>   Atomic Instruments, model 205 B (Atomic Instruments Co.,

>   Cambridge, Mass.)

>   Gain: 24   Limiting occurrs for input $\geq$ 0.2 v

Linear Amplifier:

>   Atomic Instruments, model 204 C (Atomic Instruments Co.,

>   Cambridge, Mass.)

>   Input Time Constant: 7   Feedback: 1

>   Gain: 16 (x700 amplification)
>   32 (x1200 amplification)

>   Output: High Level

Kicksorter:

>   Nuclear Data, model ND 101, (Nuclear Data Inc., Palatine,

>   California)

A.3. Electronics for $D(d,n)^3He$ Calibration

>   See Fig. 13.

Pulse Generator:

>   B.N.C. model PB-2, (Berkeley Nucleonics Co., Berkeley, Calif.)

>   Frequency: 10-100 cps   Fine Frequency: 10

>   Width: 1-10 μsec   Fine Width: 0.0

>   Polarity: negative   Amplitude: 10-560

>   Attenuator: 100   Rise Time: 0.5 μsec

Linear Amplifier:

C.I. Linear Amplifier, model # 1410, (Canberra Industries,

Middleton, Conn.)

Input Mode: neg unterm   Integration: 1

Coarse Gain: 28   Fine Gain: 7

First Differentiation: 1 Second Differentiation: off

Output: pos., unipolar, prompt

Kicksorter:

ND-160 (Nuclear Data Inc., Palatine, California)

Input: bipolar 10 v   Conversion Gain: 1024

Zero Level: 8.0   Threshold: 1.0

Coarse Gain: external amp Fine Gain: 0.0

Experimental Configuration: $\frac{1024F}{1024} \times \frac{4M}{LOW}$

Single Channel Analyzer:

C.I. Timing Single Channel Analyzer, model # 1435

(Canberra Industries, Middleton, Conn.)

Window Width: 0.94   Baseline: 0.31

Variable Delay: 0.0   Input Mode: uni

Analyzer Mode: window   Output: fast

Preamplifier and Preamplidier Input:

See A.2.